UNIVERSIDADE D
COIMBRA

Guilherme Luís João

EXPERIMENTAL CHARACTERIZATION OF A METAMATERIAL LENS FORMED BY HELICAL-SHAPED METALLIC WIRES

Projeto de dissertação no âmbito do Mestrado Integrado em Engenharia Eletrotécnica e de Computadores, área de Especialização em Telecomunicações orientado pelo Doutor Tiago André Nogueira Morgado, Doutor David Emanuel Dias Fernandes e o Doutor Sylvain Lannebère e apresentada no Departamento de Engenharia Eletrotécnica e de Computadores da Universidade de Coimbra

Julho de 2021

This work was developed in collaboration with:

Universidade de Coimbra

UNIVERSIDADE D
COIMBRA

Departamento de Engenharia Electrotécnica e Computadores

deer.uc
DEPARTAMENTO DE ENGENHARIA ELETROTÉCNICA
E DE COMPUTADORES

Instituto de Telecomunicações

instituto de
telecomunicações

UNIVERSIDADE D
COIMBRA

EXPERIMENTAL CHARACTERIZATION OF A METAMATERIAL LENS FORMED BY HELICAL-SHAPED METALLIC WIRES

Guilherme Luís João

Dissertação para obtenção do Grau de Mestre em
Engenharia Electrotécnica e de Computadores

Orientador: Doutor Tiago André Nogueira Morgado
Co-Orientador(es): Doutores David Fernandes e Sylvain Lannebère

Júri
Presidente: Doutor Henrique Leonel Gomes
Vogal: Doutor Vinícius Nunes Henrique Silva

Julho 2021

Of David.

[4] Show me your ways, LORD, teach me your paths. [5] Guide me in your truth and teach me, for you are God my Savior, and my hope is in you all day long.

- Psalm 25:4-5

Agradecimentos

Agradeço primeiramente a Deus, ao seu filho Jesus Cristo pela sua obra redentora e o privilégio de estar em sua presença.

Agradeço ao meu orientador, Doutor Tiago Morgado pela oportunidade e o privilégio da sua orientação, pelo apoio, pela dedicação, pela confiança e motivação para realização deste projeto.

Ao Doutor David Emanuel Dias Fernandes, Doutor Sylvain Lannebère e ao Doutor João de Sena Baptista Pimentel Marcos pela ajuda, por todas as sugestões e correções e por me proporcionarem um ambiente agradável de trabalho durante a realização da presente dissertação.

Ao Instituto Nacional de Gestão de Bolsa de Estudo (INAGBE) pela oportunidade, pelo apoio financeiro e por todos os meios disponibilizados para realização da minha formação em Coimbra, Portugal.

Ao Instituto de Telecomunicações (IT), e ao FCT/MCTES através de fundos nacionais e, quando aplicável, por terem financiado em parte este trabalho no âmbito do projeto UIDB/EEA/50008/2020 – HelicalMETA.

Aos meus familiares em Angola, que apesar da distância sempre me apoiaram e incentivaram bastante, por todos esforços e a amabilidade em me acompanharem ao longo destes anos com as suas palavras de encorajamento servindo sempre como uma peça fundamental para eu poder atingir os meus objetivos.

A todos os meus irmãos em Cristos, amigos e colegas que direta ou indiretamente me apoiaram para concretização deste trabalho.

A todos,
Muito Obrigado

Abstract

In 2016, it was suggested in previous work of Antennas and Propagation research group [T. A. Morgado, J. T. Costa, M. G. Silveirinha, Phys. Rev. B 93, 075102 (2016)] an alternative way to imitate the behavior of perfectly magnetic conducting (PMC) wires that can be easily implemented in the microwave regime and even at higher frequency bands. This theoretical and numerical study shows that such a metamaterial supports transverse electric mode with phase velocity nearly independent of the transverse wave vector, similar to what happens in the conventional wire medium for transverse magnetic (TM)-polarized waves.

In this thesis, using a fabricated microwave prototype, it is provided the first experimental verification of the subwavelength imaging capabilities of the helical-shaped wire medium lens. In particular, it was experimentally demonstrated that such a metamaterial slab formed by a racemic periodic array of helical-shaped metallic wires enables channeling the magnetic field components of near - field sources as predicted in the referred work. Thus, it is experimentally proven that such structure behaves indeed as a magnetic analog of the conventional wire medium lens formed by an array of parallel straight metallic wires. The proposed lens may have interesting potential applications in magnetic resonance imaging (MRI) and near-field wireless Power Transfer (NF-WPT).

Keywords

Metamaterials, wire media, canalization regime, subwavelength imaging.

Resumo

Em 2016, foi sugerido em trabalho anterior do grupo de pesquisa Antenas e Propagação [T. A. Morgado, J. T. Costa, M. G. Silveirinha, Phys. Rev. B 93, 075102 (2016)] uma forma alternativa de imitar o comportamento dos fios condutores magnéticos perfeitos (PMC) que pode ser facilmente implementada no regime de microondas e até mesmo em bandas de frequência superiores. Este estudo teórico e numérico mostra que tal metamaterial suporta um modo transversal elétrico com velocidade de fase quase independente do vetor de onda transversal, semelhante ao que acontece no meio de fio convencional para ondas transversais magneticas (TM)-polarizadas.

Nesta tese, usando um protótipo de microondas fabricado, é fornecida a primeira verificação experimental das capacidades de imagem de sub-comprimento-de-onda da lente de meio de fios em formato helicoidal. Em particular, foi demonstrado experimentalmente que a estrutura metamaterial, formada por um arranjo periódico racêmico de fios metálicos em formato helicoidal, permite canalizar as componentes do campo magnético de fontes de campo próximo conforme previsto no referido trabalho. Assim, é provado experimentalmente que tal estrutura se comporta de fato como um análogo magnético de lente de meio de fios convencionais formada por uma matriz de fios metálicos retos paralelos. A lente proposta pode ter aplicações potenciais interessantes em imagem de ressonância magnética (MRI) e transferência de energia sem fio de campo próximo (NF-WPT).

Palavras Chave

Metamateriais, wire media, regime de canalização, imaging sub-λ

Contents

List of Figures

List of Acronyms

TM transverse magnetic

TE transverse electric

DEEC Department of Electrical and Computer Engineering

PMC perfectly magnetic conducting

TEM transverse electromagnetic

CST Computer Simulation Technology

MWS Microwave Studio

VNA Vector Network Analyzer

IT Instituto de Telecomunicações

DUT Device Under Test

GUI Graphical User Interface

UV ultraviolet

MRI magnetic resonance imaging

NF-WPT near-field wireless Power Transfer

1

Introduction

Contents

1.1 Context and Motivation

Optical instruments, such as lenses, enable the control and manipulation of electromagnetic waves and are of great importance in several areas of science and technology. However, the imaging resolution of conventional lenses is limited by diffraction [1]. According to the work of Ernst Abbe [1], fine features smaller than half the wavelength of the light are not resolved by conventional lenses. This is called the diffraction limit and happens because the usual lenses cannot transport the evanescent[1] waves that carry the subwavelength details of the radiating objects.

Even though increasing the frequency of operation allows us to discriminate increasingly small details, this solution is not feasible in several contexts. For instance, when we are visualizing living organisms (e.g., biological cells), using high-frequency electromagnetic fields will lead to the death of the living samples.

Due to the increasing need to resolve deeper subwavelength details, there has been a great deal of interest in developing imaging mechanisms and technologies that enable resolutions beyond the diffraction limit. Most of the super-resolution system solutions proposed in the last decades are based on microstructured materials (designated as metamaterials) and their exotic properties [2–5].

1.1.1 Metamaterials

Metamaterials are artificially structured materials formed by properly shaped dielectric or metallic inclusions arranged in a regular lattice. The electromagnetic response of the metamaterials depends not only on the chemical composition of the constituents but, more importantly, on its geometrical arrangement [6]. Typically, the metamaterials unit cell size "a" is much smaller than the wavelength of the radiation ($a \ll \lambda$). Thus, the waves that pass through such materials can be characterized by physically meaningful homogenized constitutive parameters, i.e., effective permittivities and permeabilities [7, 8].

Similar to natural materials, in which we define permittivity and permeability by averaging out irrelevant microscopic field fluctuations at the atomic or molecular level, the homogenization models of metamaterials enable characterizing their electromagnetic responses through effective constitutive parameters. The homogenization models are accurate for effective wavelengths and averaged field variations much larger than the material granularity (long-wavelength regime) [9–11].

Complex materials with anomalous properties such as negative index of refrac-

[1] In electromagnetic theory, evanescent waves are electromagnetic waves that are spatially concentrated in the immediate vicinity of the sources and do not propagate away from the sources in usual materials

tion [12, 13], high index of refraction [14], extreme anisotropy [15], or near zero permittivity [16] have been a topic of intense research, mainly because of the possibility of overcoming the limits imposed by diffraction effects.

The following section will introduce some of the most exciting subwavelength imaging solutions based on metamaterials.

1.1.2 Subwavelength Imaging

In 2000, J. B. Pendry introduced a theoretical possibility to surpass the diffraction limit affecting conventional imaging devices. In Ref. [5], it was theoretically demonstrated that a material with negative refraction, $n = -1$, i.e., a double-negative medium with $\mu = \varepsilon = -1$, makes a perfect lens (also called "superlens"[2]) with unlimited resolution independent of the wavelength and polarization of light.

Superlens' operation is based on two distinct effects: the propagating waves are focused due to the negative refraction effect, whereas the evanescent waves are restored due to resonant excitation of surface plasmons supported by the double-negative medium.

Despite all the promising imaging potentials, some studies have pointed out a few physical constraints in obtaining high resolution with superlenses based on double-negative materials [15, 17]. Fundamental limitations are the strong sensitivity to losses and material dispersion.

In scenarios where the far-field focusing is not required and only the near-field needs to be restored, there are exciting alternatives to Pendry's lens. Significantly, in the near-field domain, the electric and magnetic responses are nearly decoupled. Consequently, only one of the constitutive parameters, μ, ε, needs to be negative [5]. Therefore, one can use materials with only negative permittivity to restore the near-field of transverse magnetic (TM)-polarized waves (or *p*-polarized waves; magnetic field parallel to the interface). Interestingly, materials with negative permittivity are naturally available at optical and ultraviolet (UV) frequencies in the form of noble metals (e.g., silver and gold). Similarly, it has been shown that artificial materials with negative permeability can be used as near-field imaging systems for transverse electric (TE)-polarized waves [18].

New ways of restoring the near-field have been proposed. One of them is found in the work of Maslovski et al., in [19], where it was shown that it is possible to use a system with two coupled planar material sheets possessing surface mode resonances to enhance the evanescent waves.

[2] In the literature, this term is often used for lenses that interact only with the near-field

Another work by Silverinha et al. proposes a new mechanism of near-field superlens based on a material formed by an ultra-dense array of nonconnected crossed metallic wires. It was theoretically proven in [20], that the subwavelength guided modes supported by such a wire metamaterial may enable the enhancement of the evanescent waves of a nearby source and the restoration of the near-field. This study was experimentally verified at microwave frequencies in [21].

An exciting alternative in the microwave, THz, and infrared regimes to the superlenses are the lenses formed by arrays of parallel metallic wires (known as "wire medium lenses") that were proposed in several works [4, 22]. These metamaterial wire lenses operate in the so-called canalization regime [3]. Such a regime relies on the transformation of almost all the source-radiation spatial spectrum (including the evanescent harmonics) into propagating waves at the input interface of the lens and its subsequent transport to the output. This is possible because of the almost flat isofrequency contours of the transverse electromagnetic (TEM) modes supported by the wire medium lenses. In Ref. [22], it was demonstrated that the wire medium lenses could transport, magnify and demagnify the near-field details with super-resolution.

One remarkable work on wire medium capable of transporting images with the subwavelength resolution is studied numerically and experimentally in [23]. In the referred work and some others reported in [22, 24], the lenses are formed by an array of parallel conducting wires. It is demonstrated that such devices can achieve subwavelength resolutions up to $\lambda/15$ and bandwidths of 18% in the microwave, THz, and infrared regimes.

Nevertheless, despite all the remarkable imaging capabilities, the wire medium lenses formed by straight parallel metallic wires have an important limitation. This kind of lenses is polarization sensitive and enables subwavelength imaging of only TM-polarized waves. For TE-polarized waves, the wire medium lenses are completely transparent because the TE waves are unable to excite currents in the wires (see figure 1.1).

An approach to overcome this polarization restriction was proposed in Ref. [25]. It was demonstrated in [25] that through the post-processing of the electric near-field transported by a titled wire medium lens, it is possible to reconstruct all the cartesian components of the near-field of the source. Although the solution reported in [25] shows that the near-field radiated from a source with an arbitrary polarization is fully restored, this strategy has some limitations. The field radiated by the relevant source needs to be stationary in time, and it is required to perform three different measurements of the electric near-field.

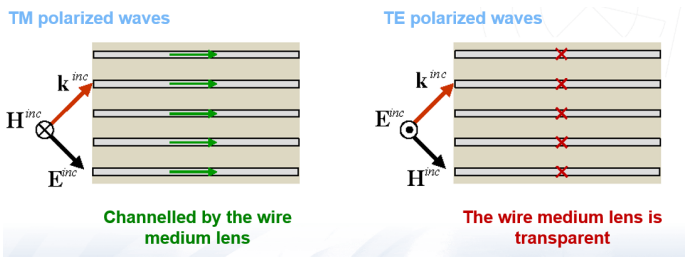

Figure 1.1: Illustration of the difference between the propagation of TM and TE polarized waves in wire medium lenses.

Achieving a canalization regime for TE-polarized waves would require replacing the metallic conducting wires with magnetic conducting wires. The problem is that there is no natural material that behaves as perfectly magnetic conducting (PMC). Hence, there is a clear need for a material with a specific and desired response beyond those found in naturally occurring materials. To realize PMC wires, one may take advantage of the exotic electromagnetic properties provided by metamaterials. A metamaterial configuration that partially mimics the response of magnetic wires is the "Swiss Rolls" [26]. It consists of a periodic array of cylinders comprising a thin conducting sheet wrapped around a central mandrel. At the resonant frequency, the Swiss Rolls lens enables the transport of a magnetic near-field distribution with a resolution limited by the roll diameter [26]. However, due to fabrication constraints, the Swiss rolls lenses are only effective at MHz frequencies.

Therefore, it turns out to be important to exploit new possibilities to mimic the response of PMC wires. A few years ago, it was theoretically proposed in the Ref. [27], that a metamaterial lens formed by a racemic [3] array of helical-shaped metallic wires that may behave as the magnetic analog of the standard wire medium lens and enable the channeling of the near-field components of TE-polarized waves.

[3] In chemistry, a racemic mixture has equal amounts of left-and-right-handed pair of enantiomers of a chiral molecule. Enantiomers are molecules that exist in the forms that are mirror images of one another but cannot be superimposed

1.2 Objectives

The objective of the dissertation is to provide the first experimental verification of the subwavelength imaging capabilities of a helical-shaped wire medium lens for TE-polarized sources. To this end, a microwave prototype of the metamaterial lens and the antenna excitation sources were fabricated. Near-field measurements of the magnetic field transported by the metamaterial lens were performed using a near-field scanning system based on a robotic arm connected to a Vector Network Analyzer (VNA).

1.3 Dissertation Outline

This thesis is organized into five chapters. This chapter introduces the thesis topic, the motivation that led to investigate and increase the knowledge in this particular topic, and describes the main strategy proposed to realize the work.

Chapter 2 describes the geometry of the metamaterial and the homogenization model that characterizes its electromagnetic response.

In chapter 3, the plane wave scattering by the metamaterial slab is studied. In the first part (Sec. 3.1), the analytical approach based on homogenization and numerical simulations is studied. Then, in Sec. 3.2, we use the full-wave simulator Computer Simulation Technology (CST) Microwave Studio (MWS) [28] to compute the scattering properties of the material numerically. Finally, in Sec. 3.3, we compare the results between the models.

Chapter 4 demonstrates that the proposed metamaterial lens may enable the transport of the subwavelength details of TE polarized waves. In Sec. 4.1, the evaluation of the lens's potentials is done by using CST MWS commercial software. Next, in Sec. 4.2.1, a brief description of the resources used to perform the required work is given. Lastly, Sec. 4.2.2, describes the experimental verification of the magnetic subwavelength field channeling using the fabricated metamaterial.

Finally, in chapter 5, the main conclusions of this work are outlined together with the perspectives for future works.

1.4 Contributions and Publications

The research presented in this thesis is part of the ongoing HelicalMETA research project (an internal Instituto de Telecomunicações (IT) project) [29] whose objectives are the demonstration of several key functionalities for the control and manipulation of light, including subwavelength imaging, sensing, and topological properties, provided by a helical-shaped wire metamaterial formed by an array of parallel metallic helices. The main contributions of this project were to deliver the first prototype of the helical-shaped wire medium lens and provide the experimental verification of its subwavelength imaging capabilities.

Subsequently, a list of the publications resulting from the research process in the scope of the thesis is presented:

1. Article in Conference

   [C.1] Tiago A. Morgado; João, Guilherme; Ricardo A. Pereira; David E. Fernandes; Sylvain Lannebère. ”Experimental Demonstration of Subwavelength Imaging using a Helical-Shaped Wire Medium Lens.” Paper presented in Conference on Telecommunications - ConfTele 2021, Leiria, 2021.

2. Journal Article

   [P.1] João, Guilherme; Tiago A. Morgado; Ricardo A. Pereira; David E. Fernandes; Sylvain Lannebère. ”Experimental Demonstration of Subwavelength Imaging using a Helical-Shaped Wire Medium Lens.” (Paper in preparation)

2

Homogenization Model

Contents

2.1 Metamaterial Geometry

The geometry of the metamaterial considered consists of a racemic periodic array of helical-shaped metallic wires oriented along the z-direction (as represented in the figure 2.1(a)[1])

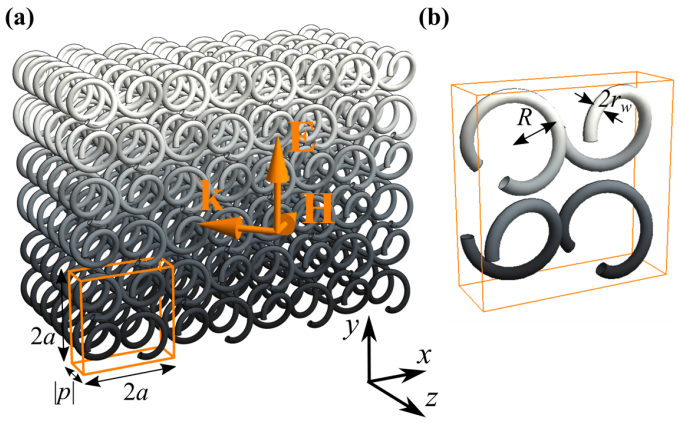

Figure 2.1: Geometry of the magnetic uniaxial wire medium: a racemic periodic array of helical-shaped metallic wires arranged in a tetragonal lattice ($a_x = a_y = 2a$ along x and y directions, and $|p|$ along the z-direction). R is the radius of helices, and r_w is the radius of the wires [30].

Each unit cell includes two right-handed helices and two left-handed helices arranged in a checkboard pattern (Fig. 2.1(b)). They stand in free space. The plane of incidence is the xoz plane and the incident wave is the TE$-z$ polarized ($\mathbf{k} = (k_x, 0, k_z^{inc}), \mathbf{E} = E^{inc}\hat{\mathbf{u}}_y$).

As illustrated in figure 2.1, the metamaterial structure is obtained by a periodic repetition of the unit cell defined by the primitive vectors $\mathbf{a}_1 = 2a\hat{\mathbf{u}}_x$, $\mathbf{a}_2 = 2a\hat{\mathbf{u}}_y$ and $\mathbf{a}_3 = |p|\hat{\mathbf{u}}_z$, where p represent the helix pitch, i.e., the height of one complete helix turn, measured parallel to the axis of the helix.

[1]Reprinted with permission of the authors

2.2 Characterization of electromagnetic response

Based on nonlocal homogenization techniques, the electromagnetic response of a metamaterial structure formed by a periodic array of helical-shaped metallic wires was originally introduced in [31] for a metamaterial structure formed by helical-shaped wires with the same handedness. Later in [27] and [32], the electromagnetic properties characterization was extended to the structure considered in this work (figure 2.1). Particularly, it was demonstrated in [27] and [32] that the electromagnetic response of such material can be characterized by the effective relative permeability and permittivity tensors $\bar{\bar{\mu}}_r$, $\bar{\bar{\varepsilon}}_r$:

$$\bar{\bar{\varepsilon}}_r = \varepsilon_t(\hat{\mathbf{u}}_x\hat{\mathbf{u}}_x + \hat{\mathbf{u}}_y\hat{\mathbf{u}}_y) + \varepsilon_{zz}\hat{\mathbf{u}}_z\hat{\mathbf{u}}_z \tag{2.1}$$

$$\bar{\bar{\mu}}_r = \hat{\mathbf{u}}_x\hat{\mathbf{u}}_x + \hat{\mathbf{u}}_y\hat{\mathbf{u}}_y + \mu_{zz}\hat{\mathbf{u}}_z\hat{\mathbf{u}}_z \tag{2.2}$$

Or equivalently

$$\bar{\bar{\varepsilon}}_r = \begin{pmatrix} \varepsilon_t & 0 & 0 \\ 0 & \varepsilon_t & 0 \\ 0 & 0 & \varepsilon_{zz} \end{pmatrix} \tag{2.3}$$

$$\bar{\bar{\mu}}_r = \begin{pmatrix} 1 & 0 & 0 \\ 0 & 1 & 0 \\ 0 & 0 & \mu_{zz} \end{pmatrix} \tag{2.4}$$

With

$$\varepsilon_{zz} = 1 - \frac{1}{\frac{k_0^2}{\beta_{p1}^2} - \frac{k_z^2}{\beta_{p2}^2}} + \frac{A^2k_0^2}{\left(1 + \frac{A^2k_0^2}{\frac{k_0^2}{\beta_{p1}^2} - \frac{k_z^2}{\beta_{p2}^2}}\right)\left(\frac{k_0^2}{\beta_{p1}^2} - \frac{k_z^2}{\beta_{p2}^2}\right)^2} \tag{2.5}$$

$$\mu_{zz} = \frac{1}{\left(1 + \frac{A^2k_0^2}{\frac{k_0^2}{\beta_{p1}^2} - \frac{k_z^2}{\alpha\beta_{p2}^2}}\right)} \tag{2.6}$$

$$\varepsilon_t = \varepsilon_{xx} = \varepsilon_{yy} = 1 + \frac{(\pi R)^2}{V_{cell}}\frac{1}{C_1} \tag{2.7}$$

$$\beta_{p1} = \sqrt{\frac{(2\pi p)^2}{C_0 p^2 V_{cell} + 8C_1\pi^2R^2V_{cell}}} \tag{2.8}$$

$$\beta_{p2} = \sqrt{\frac{(2\pi)^2}{C_0 V_{\text{cell}}}} \tag{2.9}$$

In the above expressions, $A = \frac{\pi R^2}{|p|}$, α is a correction factor, $V_{\text{cell}} = a^2|p|$ is the volume of the unit cell, β_{p1} and β_{p2} are wave number parameters that only depend on the geometry of the material and whose definitions (as well as C_0 and C_1 parameters definitions) can be found in [27, 31, 32].

Equations (2.3-2.6) establish that the effective medium behaves as a uniaxial non-bianisotropic magneto-dielectric material with an optical axis along z-direction. Moreover, the relative permittivity and permeability tensors of the effective medium are frequency dispersive and spatially dispersive (or nonlocal). It is clearly seen from (2.2-2.6) that the axial (i.e., along the z-direction) permittivity and permeability depend explicitly on the z component of the wave vector, k_z.

One should note that for the particular case where β_{p2} is much greater than k_z, ($\beta_{p2} \gg k_z$), the relative permittivity and permeability tensors, $\bar{\bar{\varepsilon}}_r$ and $\bar{\bar{\mu}}_r$, become solely frequency-dependent, since the term $\frac{k_z^2}{\beta_{p2}^2}$ in their expressions can be discarded. In this case, the electromagnetic response of the metamaterial is local, and the dielectric tensor is anisotropic [2] and indefinite [3].

2.2.1 Dispersion characteristics of the TE-z polarized waves

This section will study the dispersion properties of the plane waves supported by the considered helical wire medium. In particular, we will focus our analysis on the study of the TE-z planes waves (with electric field parallel to the *xoy* plane; see figure 2.1). The dispersion of the TE waves in this metamaterial is given by [31]:

$$k_0^2 \varepsilon_t - \frac{1}{\mu_{zz}} k_t^2 - k_z^2 = 0 \tag{2.10}$$

Where $k_t^2 = k_x^2 + k_y^2$, ε_t is defined by the equation (2.7) and μ_{zz} is given by the equations (2.6).

The equation (2.10) can be reduced to a second-order degree polynomial in the variable k_z^2:

$$k_z^4 \beta_{p1}^2 + k_z^2 \left(k_x^2 \beta_{p1}^2 - k_0^2 \varepsilon_t \beta_{p1}^2 - k_0^2 \alpha \beta_{p2}^2\right) - k_0^2 \left(A^2 \alpha \beta_{p1}^2 \beta_{p2}^2 k_x^2 + \alpha \beta_{p2}^2 k_x^2\right) + k_o^4 \varepsilon_t \alpha \beta_{p2}^2 = 0 \tag{2.11}$$

[2] Unlike isotropic materials, whose properties are identical in all directions, anisotropic material's properties change with the direction along with the structures

[3] Indefinite media are anisotropic media for which not all components of the permittivity and/or permeability tensors have the same sign

Thus, the homogenization model predicts that the structured medium supports two independent plane waves, i.e., for a fixed frequency, it supports two independent eigenmodes associated with an electric field (along y-direction). This is a consequence of the nonlocal response of the material [27, 31, 32]. Note that standard local materials support a single electromagnetic mode for each fixed polarization.

The isofrequency contours associated with the two TE modes supported by the considered metamaterial are illustrated in fig. (2.2). From this figure, one can see that one of the modes is hyperbolic, and the other is elliptical.

For the same TE polarization and arbitrarily long-wavelengths (low frequencies), both hyperbolic and elliptical modes propagate simultaneously in the metamaterial structure. This is a very unusual characteristic, since in standard media or even in the vast majority of the known metamaterial structures, for a fixed wave polarization and at low frequencies, only an electromagnetic mode propagates. For this reason, the helical-wire medium is somehow fascinating since, in this metamaterial, two modes coexist and propagate even for long-wavelengths.

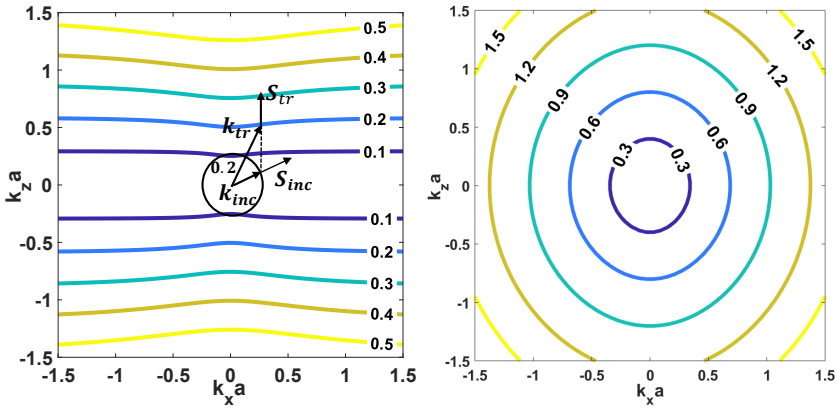

Figure 2.2: Isofrequency contour of the two TE plane waves modes for propagation in the xoz plane with electric field perpendicular to it. (left: hyperbolic-type modes; right: elliptical-type modes). The number insets specify the value of $\omega a/c$ associated with each curve.

The isofrequency contours of the hyperbolic mode are almost flat so that k_z is nearly independent of k_x (see Fig. 2.2). One can observe that the energy inside the metamaterial slab always flows along the axial direction of the helices, i.e., the Poynting vector is directed mostly along z, and it is almost independent of the transverse wave number, k_x, both for propagating waves ($k_x < k_0$) and for evanescent waves ($k_x > k_0$) [27, 30]. Thus, this indicates that the hyperbolic mode supported by the helical-shaped wire metamaterial may enable a canalization regime for TE-z polarized waves, analogous to the standard wire medium for TM-polarized waves.

3

Transmission Properties

Contents

In this chapter, the transmission properties of the metamaterial slab formed by helical-shaped wires are studied under plane wave incidence using the nonlocal homogenization model (Sec. 3.1) and full-wave simulations obtained with the electromagnetic simulator [28] (Sec. 3.2).

3.1 Analytical Approach based on the homogenization model

To begin with, the attention is focused on studying the simple plane wave scattering problem using the nonlocal homogenization model introduced in the previous section. The metamaterial slab is assumed infinite and periodic along the x and y directions with lattice periods $a_x = 2a$ and $a_y = 2a$, respectively, and finite with thickness L along the z-direction (figure 2.1). The incident wave vector belongs to the xoz plane ($k_y = 0$). Thus, the electric field in the three regions of space can be written as follows (the x dependence and the time variation $e^{j\omega t}$ are suppressed):

$$\begin{cases} E_y^{(1)} = E_y^i(e^{\gamma_0 z} + \rho e^{-\gamma_0 z}), & z > 0 \\ E_y^{(2)} = A_1^+ e^{-jk_z^{(1)} z} + A_1^- e^{+jk_z^{(1)} z} + A_2^+ e^{-jk_z^{(2)} z} + A_2^- e^{+jk_z^{(2)} z}, & -L < z < 0 \\ E_y^{(3)} = E_y^i T e^{\gamma_0 (z+L)}, & z < -L \end{cases} \quad (3.1)$$

where E_y^i is the incident electric field, $\gamma_0 = \sqrt{k_x^2 - \omega^2 \varepsilon_0 \mu_0}$ is the free space propagation constant, $k_x = \omega\sqrt{\varepsilon_0\mu_0}\sin\phi$ (ϕ is the angle of incidence), and ρ and T are the reflection and transmission coefficients, respectively. The propagation constants, $k_z^{(1,2)}$ are calculated using equation (2.11) and the amplitudes $A_{1,2}^{\pm}$ are associated with the two TE modes excited inside the metamaterial slab.

For each plane wave with the electric field of the form $\mathbf{E} = E_0 e^{-j\mathbf{k}.\mathbf{r}}\hat{\mathbf{u}}_y$ the corresponding magnetic field outside metamaterial is given by:

$$\mathbf{H} = \frac{E_0}{\mu_0 \omega}(\mathbf{k} \times \hat{\mathbf{u}}_y) \quad (3.2)$$

Using some relations and applying the Maxwell-Faraday equation, one can write:

$$\mathbf{H} = \frac{E_0}{k_0 \eta_0}(-k_z \hat{\mathbf{u}}_x + k_x \hat{\mathbf{u}}_z)\, e^{-j\mathbf{k}.\mathbf{r}} \quad (3.3)$$

Similarly, the corresponding magnetic field inside metamaterial is given by:

$$\mathbf{H} = \frac{E_0}{\mu_0 \omega} \bar{\bar{\mu}}_r^{-1} \cdot (\mathbf{k} \times \hat{\mathbf{u}}_y) \quad (3.4)$$

We can derive the following equation:

$$\mathbf{H} = \frac{E_0}{\mu_0 \omega}\left(-k_z \hat{\mathbf{u}}_x + \frac{k_x}{\mu_{zz}} \hat{\mathbf{u}}_z\right) e^{-j\mathbf{k}.\mathbf{r}} \quad (3.5)$$

One can use the equations (3.3) and (3.5) to write the expression for the magnetic field in all regions, similar to the equation (3.1) for the electric field.

To calculate the transmission and reflection coefficients it is required to impose that the tangential components of the electromagnetic fields (E_y and H_x) are continuous at the interfaces $z = 0$ and $z = -L$ (classical boundary condition). However, since two plane waves coexist in the metamaterial, classical boundary conditions are insufficient to determine all the unknowns of the scattering problems equation. In particular, it is necessary to impose that the z-component of the magnetic field is continuous at both interfaces (ABC condition) [27].

This ABC condition can be seen as the magnetic counterpart of the ABC condition applied in the standard wire medium formed by parallel metallic wires [33]. The ABC enables us to accurately model the effects of spatial dispersion and the behavior of the microscopic currents flowing along the helically shaped wires

Using the usual and ABC conditions, we obtain a 6x6 linear system of equations that can be solved numerically using, for example, Matlab [34].

3.2 Full-Wave numerical simulation using CST Microwave Studio

To numerically calculate the scattering properties of the material, it was used the full-wave simulator CST MWS [28].

Since computers can only solve problems in limited space for electromagnetic calculation or electromagnetic simulation analysis, one needs to specify the boundaries conditions. CST MWS uses computational domain of cuboid shape (the bounding box). As depicted below, there can be six different boundaries surfaces at the minimum and maximum position in each coordinate direction.

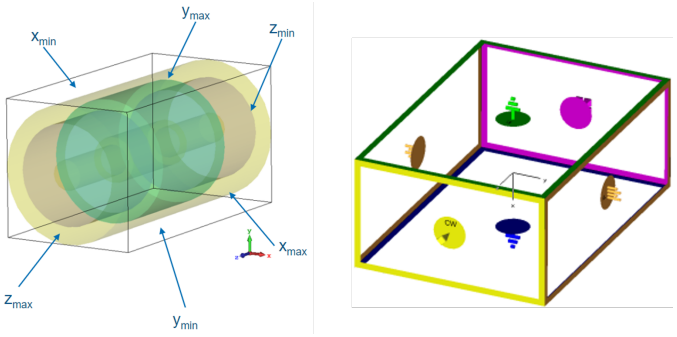

Figure 3.1: CST MWS boundary conditions [28].

To this end, it was considered a unit cell of the proposed metamaterial, and it was specified the periodic boundaries conditions along x and y direction due to the nature of the structure (figure 3.2). Because the structure is infinitely periodic along the x- and y- coordinates, we only need to consider a structure corresponding to a partial period of the metamaterial along with such directions. The excitation ports are placed in the z-direction.

In order to calculate transmission coefficient, T, as a function of the transverse component of the wave vector, k_x, it is required to define the phase shift, ϕ, in the periodic boundary condition along x-direction as follow:

$$\phi = \frac{180}{\pi} k_{rat} k_0 a_x \tag{3.6}$$

where $k_0 = \frac{2\pi f}{c}$, $a_x = 2a$ and $k_{rat} = \frac{k_x}{k_0}$.

The phase shift comes from the Bloch-Floquet theory for periodic systems, which states that the electromagnetic fields at a given point x and at a point $x+X$, where $X = 2a$ is the dimension of the unit cell, differ only from one phase factor of e^{-jk_xX}. Frequency solver was used, and a parameter sweep was run for k_{rat}.

To guarantee accurate discretization of the structure, it was defined and refined the hexahedral mesh. It is important to refer that, in CST MWS, the accuracy and

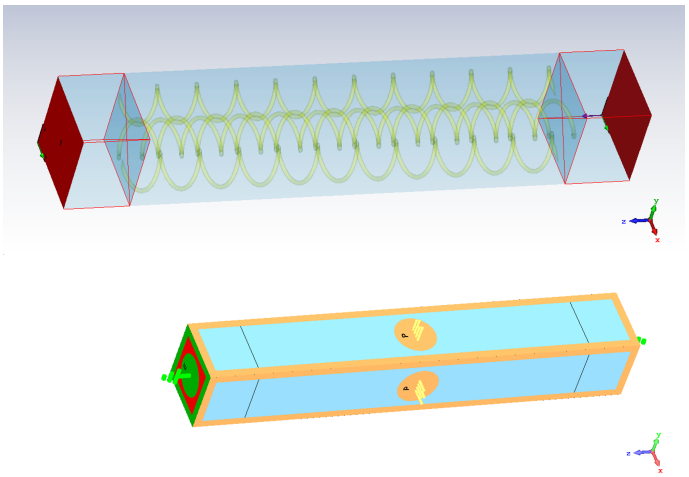

Figure 3.2: Design of the unit cell of the metamaterial in CST Microwave Studio. (Top: 3D representation of the design; Bottom: Specification of boundary and symmetries condition)

performance of a simulation are heavily dependent on the quality of the mesh which describes the structure. Nevertheless, sophisticated mesh refinement may lead to exaggerated computational complexity, which may lead to non-converging simulations. Thus, it is important to find a balance between the complexity of the simulation and the quality of the numerical results.

3.3 Transmission coefficient results

In this section, the magnitude of the transmission coefficient as a function of the k_x calculated using the effective model (solid lines) and through the CST simulations (discrete symbols) are presented. As seen from Fig. 3.3, apart from the slight frequency shift in the effective medium model results (the frequencies are about 15.8% higher than the values used in the full-wave simulations), the agreement between them is very satisfactory.

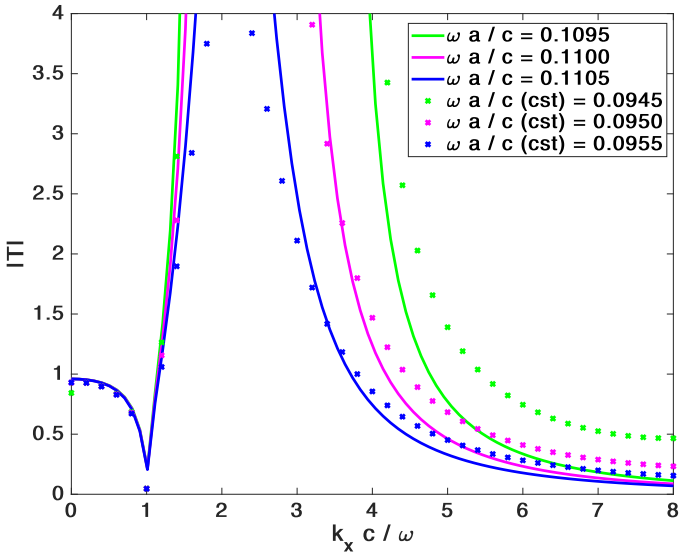

Figure 3.3: Amplitudes of the transmission coefficients as a function of the normalized k_x using a fixed thickness $L = 10a$ of the slab for different frequencies of operations. Solid lines: nonlocal homogenization results; Discrete symbols: full wave results [28]. The set of parameters values used in the effective medium model are: $\varepsilon_h = 1, R = 0.4, a = 1; r_w = 0.05, p = 0.9, C_0 = 3.046941, C_1 = 2.236693$ and $\alpha = 0.51$.

One can see from the figure that, for propagating waves, $k_x\omega/c \leq 1$, the transmission coefficient is close to unity. Moreover, both models predict that $|T| \geq 1$ for a significant part of the spectrum of the evanescent waves (up to about $k_x = 5 \cdot k_0$). Somewhat analogous to the standard wire medium formed by straight metallic wires for TM-polarized waves, Fig. 3.3 predicts that the helical-shaped wire medium operates in a canalization regime and is capable of transporting subwavelength details of TE polarized waves.

4

Near-Field Imaging

Contents

This chapter demonstrates through simulation and experimental work that the proposed metamaterial lens may enable indeed the transport of the subwavelength details of TE polarized waves.

4.1 Simulation of the electromagnetic response using CST

We will begin evaluating the potentials of near-field imaging of the helical-shaped wire medium lens using CST MWS commercial software [28].

We designed a helical-shaped wire medium lens with a spatial period of $2a = 10$ mm, $R = 0.4a = 2$ mm, $r_w = 0.05a = 0.25$ mm, $|p| = 0.9a = 4.5$ and dimensions $L_x = L_y = 36a = 180$ mm along the x and y directions and $L = 10a = 50$ mm along the z direction (see figures 4.1 and 4.12). We consider a scenario wherein the metamaterial is illuminated by the small near-field magnetic loops, which are disposed of in the form of square and parallel to the interface plane. The currents feeding the loops are in phase.

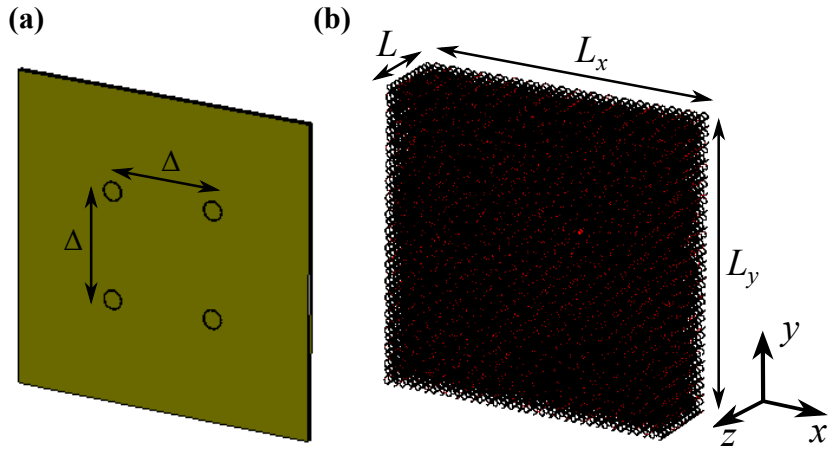

Figure 4.1: Geometries of the prototypes. (a) Excitation source; (b) Finite-sized magnetic wire medium lens.

We simulated the electromagnetic response of the finite-sized magnetic wire medium lens (figure 4.1b) composed of helical-shaped copper (C_u) wires in CST MWS [28]. Since in this case we have a finite structure, open boundary conditions were used to ensure that waves can pass this boundary with minimal reflections and the simulation was done considering the transient solver. The four near-field magnetic loops illuminate the lens (figure 4.1a) are placed at distance $d_1 = a = 5$ mm from the front interface. Next, the figures with the time snapshots obtained from the electromagnetic simulator CST [28].

Figures below show the time snapshots of the normalized z-component of the magnetic field, H_z, at the source and image planes. As it is seen in the figures 4.2b, 4.3b and 4.4b, despite the distance between the loops being subwavelength ($\Delta = \lambda_0/4$, $\Delta = \lambda_0/6$ and $\Delta = \lambda_0/8$), the four loops are perfectly discernible from one another at the image plane.

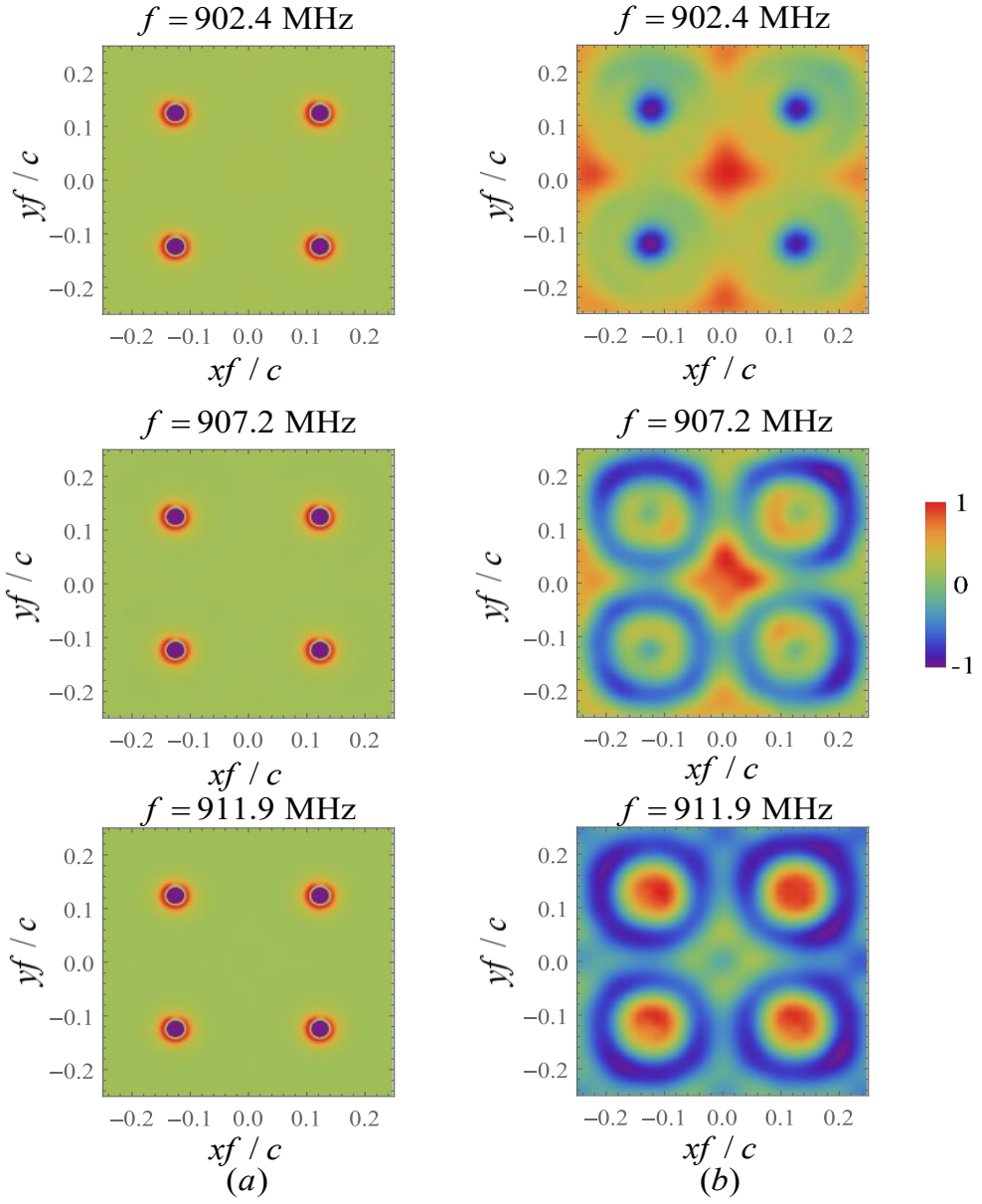

Figure 4.2: CST MWS results of the normalized magnetic field component, $H_z(t = 0)$ for three different frequencies and $\Delta = \lambda_0/4$ (relative to central frequency of 907.2 MHz). (a) Source plane, at a distance of 5 mm from both the front interface and the source. (b) Image plane, at a distance of 2.5 mm from the back interface.

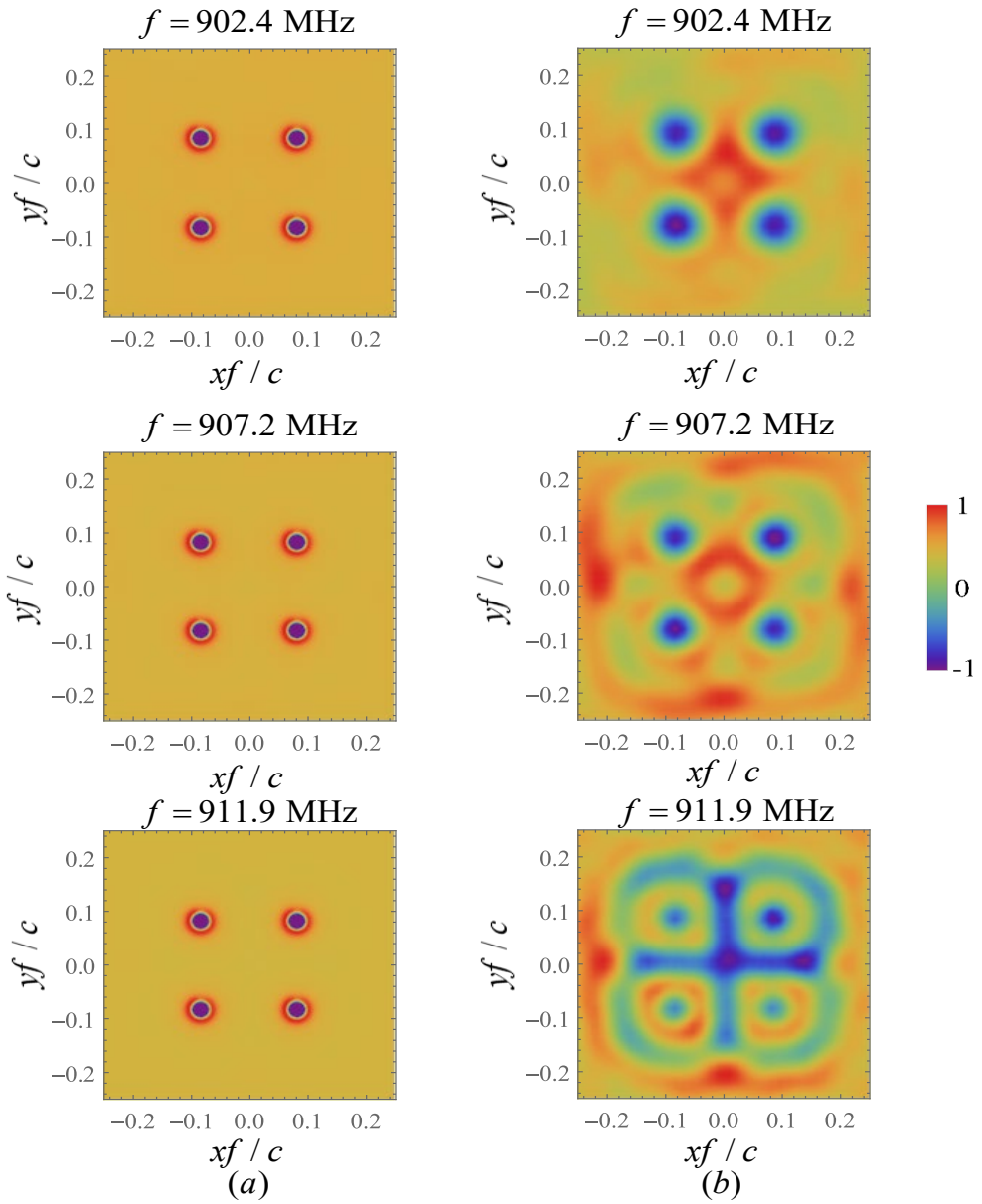

Figure 4.3: CST MWS results of the normalized magnetic field component, $H_z(t = 0)$ for three different frequencies and $\Delta = \lambda_0/6$ (relative to central frequency of 907.2 MHz). (a) Source plane, at a distance of 5 mm from both the front interface and the source. (b) Image plane, at a distance of 2.5 mm from the back interface.

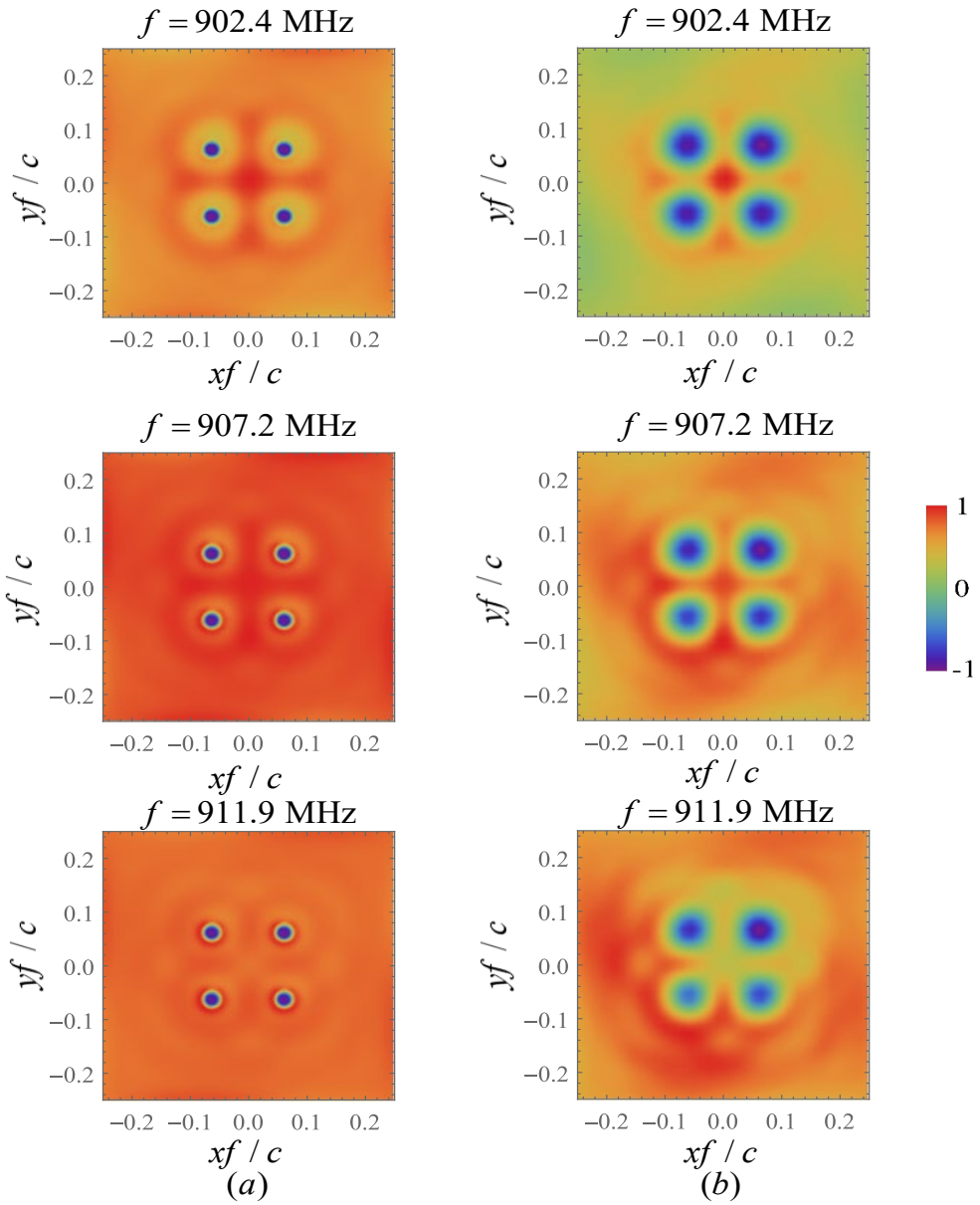

Figure 4.4: CST MWS results of the normalized magnetic field component, $H_z(t = 0)$ for three different frequencies and $\Delta = \lambda_0/8$ (relative to central frequency of 907.2 MHz). (a) Source plane, at a distance of 5 mm from both the front interface and the source. (b) Image plane, at a distance of 2.5 mm from the back interface.

The density plot of the magnetic field amplitude $|\mathbf{H}_z|$ for $f = 911.9$ MHz in the plan *yoz* obtained with CST MWS is depicted below. In this figure, one can see the channeling effect, which enables the near-field of the loops to be transported to the image plane.

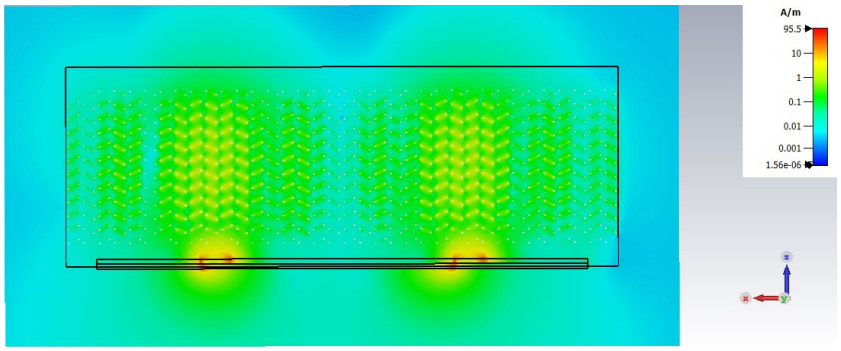

Figure 4.5: Top view of the amplitude of magnitude field $|\mathbf{H}|$ for $f = 911.9$ MHz in the plane *yoz* with the same geometrical parameters as above.

4.2 Experimental Verification

4.2.1 Experimental measurement resources

The measurements of the proposed system were done using the near-field scanning system available at the Microwave Laboratory in the Department of Electrical and Computer Engineering (DEEC), in the IT of Coimbra. The system consists of a robotic arm with a round shielded loop probe connected to a VNA, illustrated in the figure 4.6 [1].

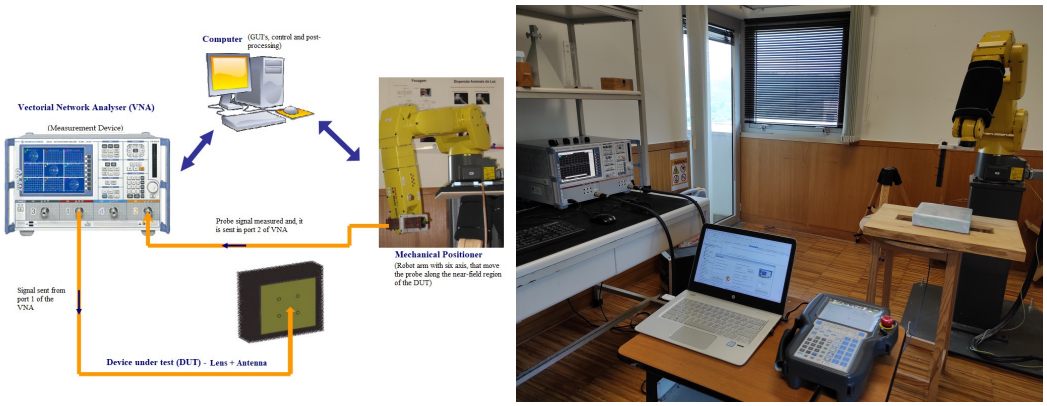

Figure 4.6: (Left) Near-Field measurements system structure (adapted) [35]. (Right) Photo of the near-field measurements system of Microwave Laboratory of the IT-Coimbra.

4.2.1.A Vector Network Analyzer - VNA

One of the main components of the measurement system is the VNA. VNAs enable measuring the network parameters of electrical networks. They test component specifications and verify design simulations to make sure systems and their components work properly together [36].

The following figure illustrates how VNAs work. A stimulus signal is injected into the Device Under Test (DUT), and the VNA measures both the signal reflected from the input side and the signal that passes through the DUT to the output side. Next, the results from the measurements are processed and then displayed (figure 4.7)

VNAs perform two types of measurements – transmission (S21, S12, gain, insertion loss/ phase, electrical length/delay, etc.) and reflection (S11 and S22).

The VNA model used in the measurements is the Rohde & Schwarz ZVB 20 (with a bandwidth of 10 MHz up to 20 GHz), shown in the figure .4.8

[1] 1

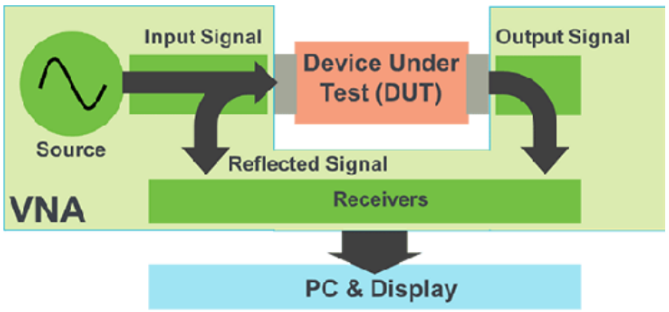

Figure 4.7: Basic Operation of VNA [36].

Figure 4.8: VNA with the calibration kit

In the experimental work, we use VNA to measure the amplitude and phase of the S21 parameter, which is directly related to the transmitted field by the lens.

4.2.1.B Mechanical Positioner

To move the probe along the scanning area, we use an industrial robotic arm that performs efficient repeated measures with a good spatial resolution. As is illustrated in the figure 4.9, the laboratory of Microwave IT-Coimbra is equipped with a robotic arm, FANUC LR Mate 200iC 5L, along with its controller, FANUC R-30iA Mate.

Next, the loop sensor, used as a magnetic field probe, is shown. This probe fabricated in the Microwave Laboratory of IT-Coimbra enables measuring the magnetic field with good resolution.

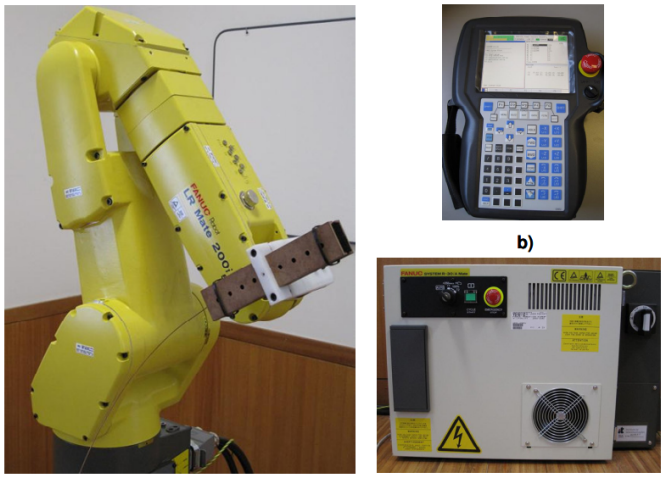

Figure 4.9: (a) Robot - FANUC LR Mate 200iC 5L. (b) Console for Manual control and activation functionality (c) Controller - FANUC R-30iA Mate. [35].

Figure 4.10: Magnetic field probe.

4.2.1.C Control Software - IT Near-Field Scanner

The software used to control the system is called “IT Near-Field Scanner” developed in C++ language with four main components [35].

- Graphical User Interface (GUI): Enables the configuration of different system parameters.
- Robot Controller: Provides functions with instructions that are sent to the robot arm to perform the required task of scanning
- VNA Controller: Provides control functions that perform management of every request and answer of the parameter to be measured.
- Post-Processing unit: Enables the data’s management and processing functions to guarantee fast manipulation and visualization.

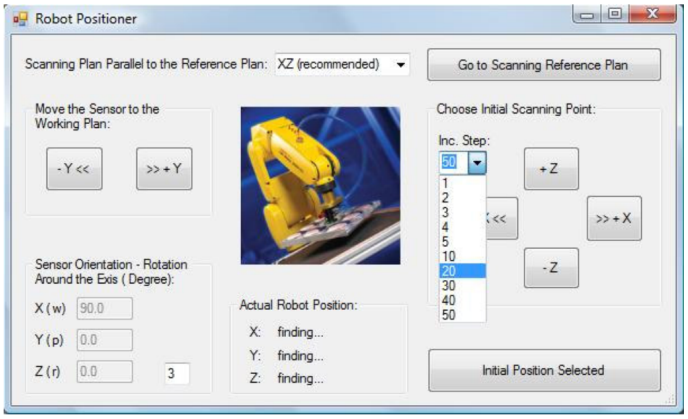

Figure 4.11: Robot Positioner window that transports the probe to the initial position to start the scanning.

4.2.2 Experimental Results

We fabricated a helical-shaped wire medium lens prototype to experimentally verify the possibility of magnetic subwavelength field channeling. The metamaterial lens prototype consists of an array of 36x36 helical-shaped steel wires (specifically, 648 right-handed helical-shaped wires and 648 left-handed helical-shaped wires) arranged in a checkerboard pattern. As seen in 4.12, the helical-shaped wires are embedded in a styrofoam block whose relative permittivity is close to unity around the design frequency.

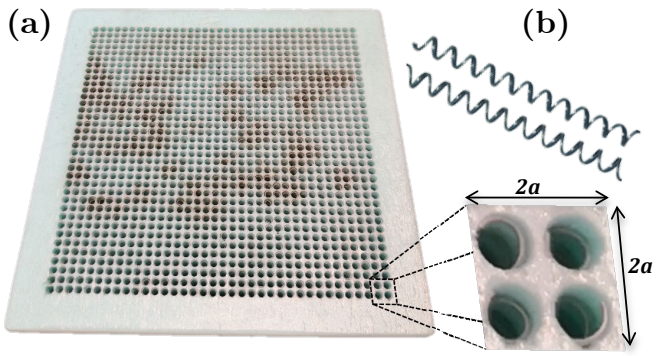

Figure 4.12: (a) Photo of the prototype of the racemic helical-shaped wire medium lens; (b) Left- and Right-handed helical-shaped wires.

We have also designed and simulated several excitation antennas that possess sub-wavelength details. To this end, we have considered a set of four planar magnetic loops in a square disposition. We fabricated the excitation source using standard printed circuit technology (see figure 4.13). Each loop has 10 mm of diameter, and we separated them by a subwavelength distance of delta Δ.

The experimental time snapshots of the normalized z-component of the magnetic field obtained from the near-field measurements are shown in Figs. 4.14, 4.15

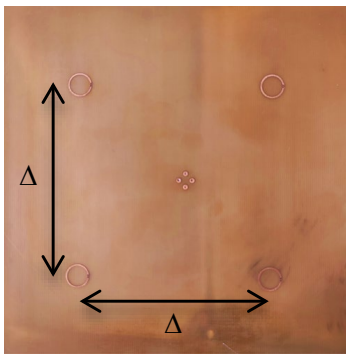

Figure 4.13: Photo of the excitation antenna array fabricated using the standard printed circuit board, formed by four small magnetic loops

and 4.16).

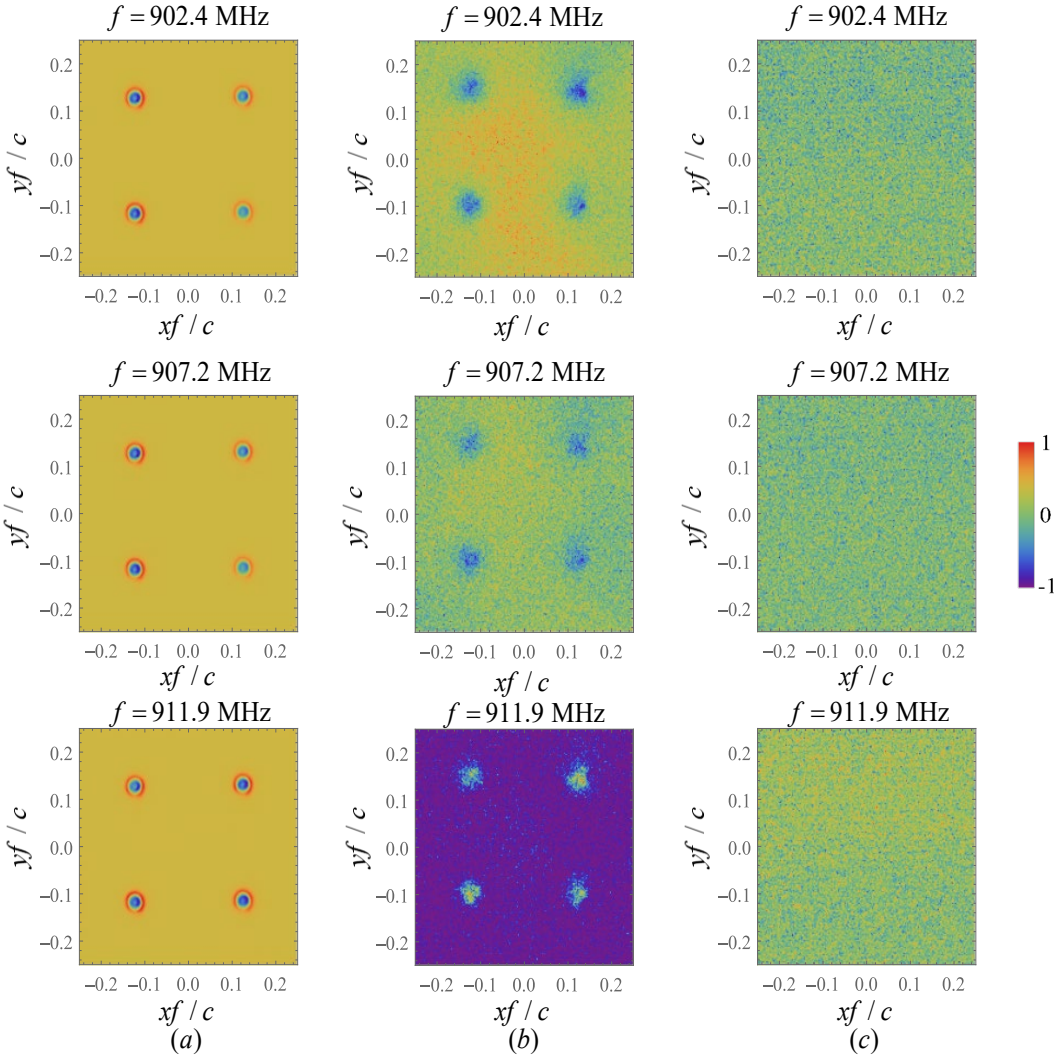

Figure 4.14: Experimental results of the normalized magnetic field component, $H_z(t=0)$ for three different frequencies and $\Delta = \lambda_0/4$ (relative to central frequency of 907.2 MHz). (a) Without lens (source plane - 2.5 mm from the loops); (b) At image plane (a/2=2.5 mm above the output interface of the lens); (c) at the same plane as in (b) but in the absence of the metamaterial lens.

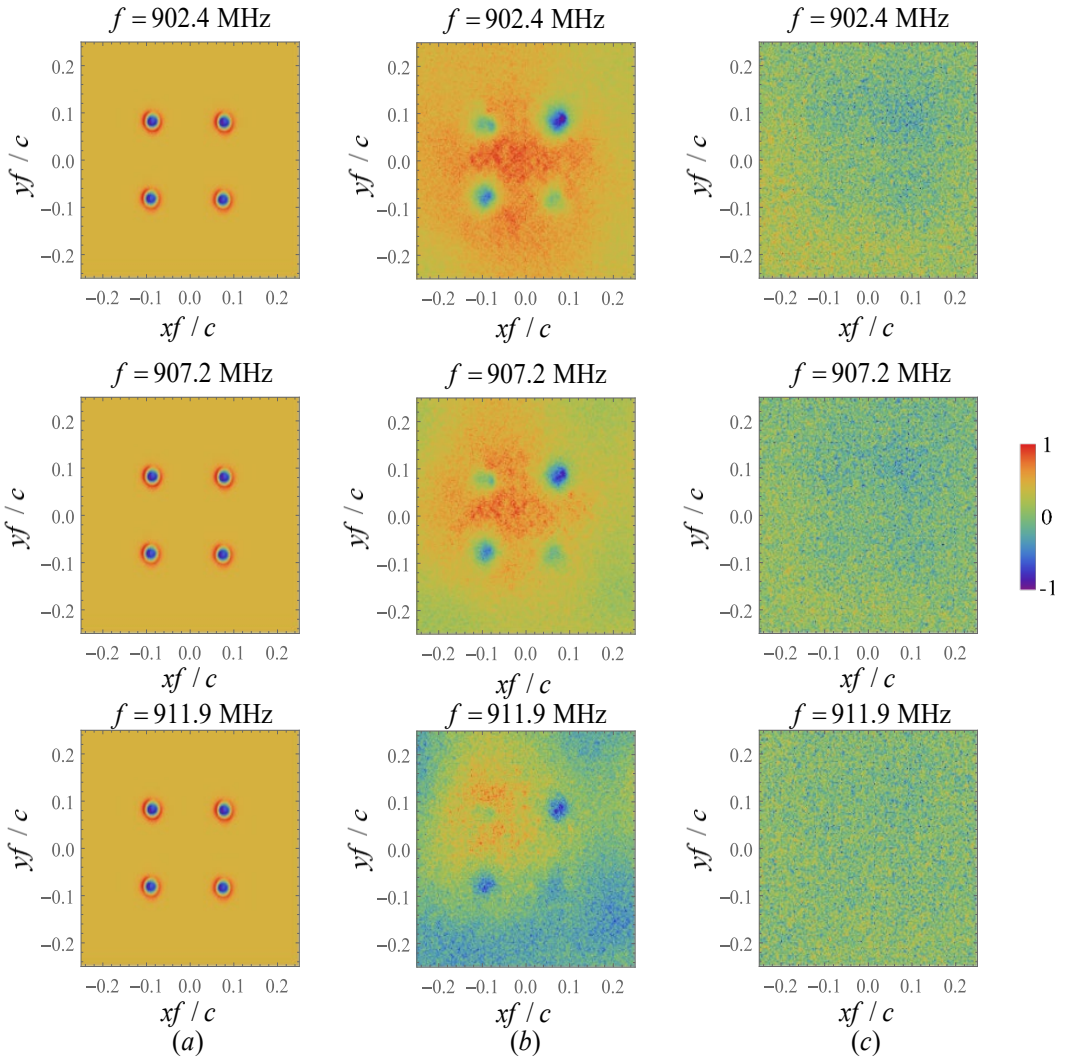

Figure 4.15: Experimental results of the normalized magnetic field component, $H_z(t=0)$ for three different frequencies and $\Delta = \lambda_0/6$ (relative to central frequency of 907.2 MHz). (a) Without lens (source plane - 2.5 mm from the loops); (b) At image plane (a/2=2.5 mm above the output interface of the lens); (c) at the same plane as in (b) but in the absence of the metamaterial lens.

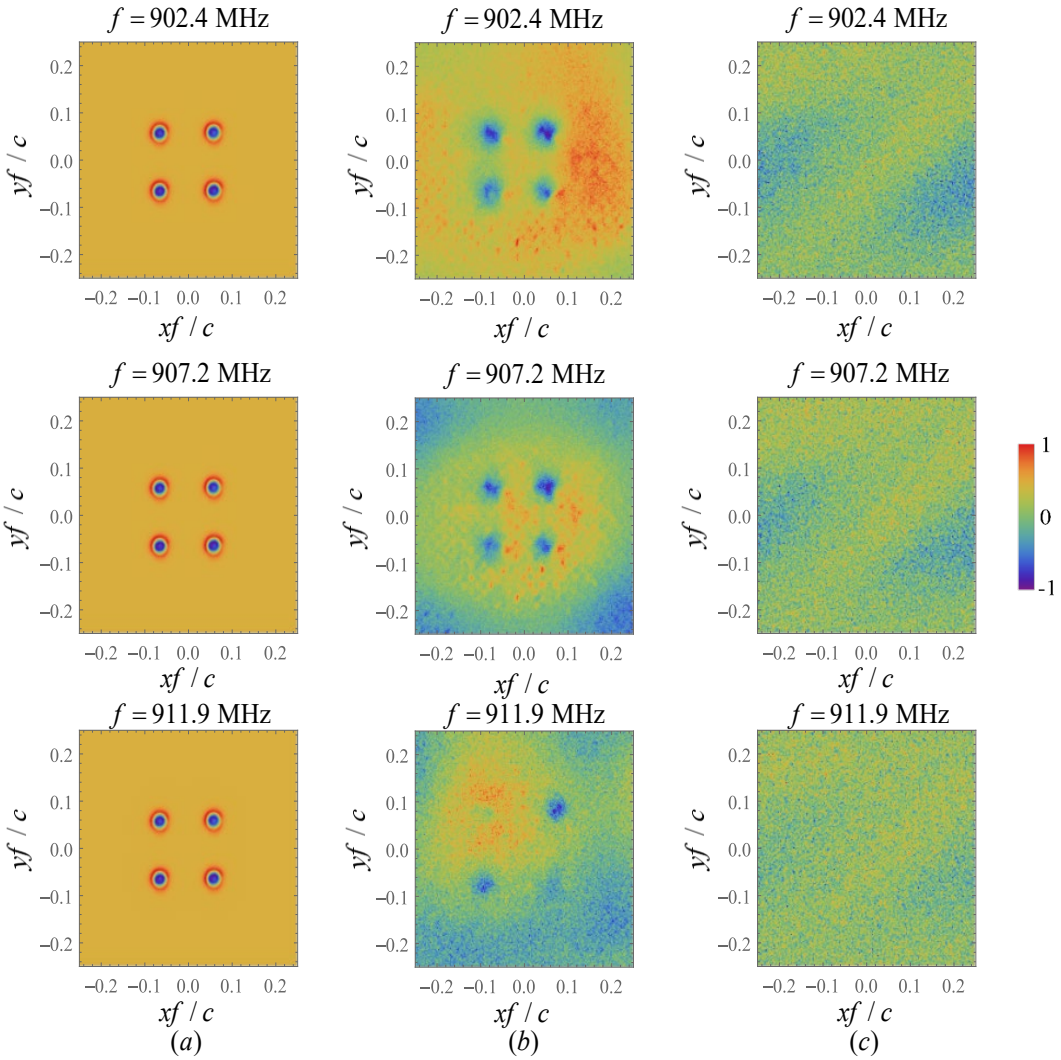

Figure 4.16: Experimental results of the normalized magnetic field component, $H_z(t=0)$ for three different frequencies and $\Delta = \lambda_0/8$ (relative to central frequency of 907.2 MHz). (a) Without lens (source plane - 2.5 mm from the loops); (b) At image plane (a/2=2.5 mm above the output interface of the lens); (c) at the same plane as in (b) but in absence of the metamaterial lens.

One can see clearly from the figures above (Figs. 4.14, 4.15 and 4.16) that when the metamaterial lens is present in between the excitation source and the probe, similar to the result obtained with the CST, the four magnetic loops are perfectly resolved from each other at the image plane. This is only possible because of the channeling of the magnetic near-field of the loops by the metamaterial lens. Quite differently, the radiation of the near-field loops is completely imperceptible at the image plane when the lens is removed.

One can see from the results of the excitation source with $\Delta = \lambda_0/4$, that the radiation of the loops in the image plane is more symmetric than for the other antennas with $\Delta = \lambda_0/6$ and $\Delta = \lambda_0/8$. These differences are due to the fact that the four loops may not all be at the same distance from the input interface of the lens. This is so because the boards of the printed antennas became slightly curved during the fabrication process. Note that since the loops are near-field radiators, even minimal distance differences can cause considerable asymmetries in the amplitude of the loops field at the image plane. The boards of the printed antenna with $\Delta = \lambda_0/4$ is the straighter one, which explains why the field of the four loops at the image plane is more symmetric in this case.

5

Conclusions

Contents

In this thesis, the subwavelength imaging capabilities of a helical-shaped wire medium lens were theoretically and experimentally investigated. It was experimentally demonstrated that the nearly flat isofrequency contours of the hyperbolic mode enable indeed a canalization regime for TE-polarized waves. The racemic helical-shaped wire medium behaves as a magnetic analog of the conventional wire medium formed by straight metallic wires. Therefore, we have experimentally validated the concept of magnetic near-field channeling using a fabricated microwave prototype of a metamaterial lens formed by a racemic array of helical-shaped metallic wires, introduced by the IT-Coimbra research group in [27].

These studies may be useful for the development of novel microwave and terahertz imaging devices. The proposed lens may have interesting potential applications in magnetic resonance imaging (MRI), in the sense that the resolution of MRI images may be substantially improved through the use of these metamaterials.

The magnetic near-field channeling provided by the helical-shaped wire medium lens mays be also quite useful in near-field wireless Power Transfer (NF-WPT) applications.

5.1 Future Work

Although quite interesting results were achieved using the excitation antenna array formed by the four small magnetic loops, one of the future possibilities is to test the response of the helical-shaped wire medium lens with other kinds of magnetic near-field sources. Another work that we plan to develop soon is to study the electromagnetic response of a nested wire medium formed by a racemic array of helical-shaped metallic wires interlaced with an array of straight metallic wires.

Some other future works may involve subwavelength imaging on thicker lenses tuned to higher Fabry-Perot resonances.

Bibliography

[1] E. Abbe, "Beiträge zur theorie des mikroskops und der mikroskopischen wahrnehmung," *Archiv für Mikroskopische Anatomie*, vol. 9, no. 1, pp. 413–468, Dec 1873. [Online]. Available: https://doi.org/10.1007/BF02956173

[2] X. Zhang and Z. Liu, "Superlenses to overcome the diffraction limit," *Nature materials*, vol. 7, pp. 435–41, 07 2008.

[3] P. Belov, Y. Hao, and S. Sudhakaran, "Subwavelength microwave imaging using an array of parallel conducting wires as a lens," *Phys. Rev. B*, vol. 73, p. 033108, 01 2006.

[4] M. Silveirinha, P. Belov, and C. Simovski, "Sub-wavelength imaging at infrared frequencies using an array of metallic nanorods," *Physical Review B*, vol. 75, 10 2006.

[5] J. Pendry, "Negative refraction makes a perfect lens," *Physical review letters*, vol. 85, pp. 3966–9, 11 2000.

[6] C. Simovski, P. Belov, A. Atrashchenko, and Y. Kivshar, "Wire metamaterials: Physics and applications," *Advanced materials (Deerfield Beach, Fla.)*, vol. 24, pp. 4229–48, 08 2012.

[7] M. Silveirinha, "A metamaterial homogenization approach with application to the characterization of microstructured composites with negative parameters," *Physical Review B*, vol. 75, 12 2006.

[8] C. Simovski and S. Tretyakov, "Local constitutive parameters of metamaterials from an effective-medium perspective," *Phys. Rev. B*, vol. 75, pp. 195 111–10, 05 2007.

[9] D. Smith and J. Pendry, "Homogenization of metamaterials by field averaging (invited paper)," *JOSA B*, vol. 23, 03 2006.

[10] A. Alù, "First-principle homogenization theory for periodic metamaterials," *Phys. Rev. B*, vol. 84, 12 2010.

[11] S. Lannebère, T. A. Morgado, and M. G. Silveirinha, "First principles homogenization of periodic metamaterials and application to wire media," *Comptes Rendus Physique*, 02 2020.

[12] Z. Jaksic, N. Dalarsson, and M. Maksimovic, "Negative refractive index metamaterials: Principles and applications," *Microwave Review*, vol. 12, 04 2006.

[13] D. Smith, W. Padilla, D. Vier, S. Nemat-Nasser, and S. Schultz, "Composite medium with simultaneously negative permeability and permittivity," *Physical Review Letters*, vol. 84, p. 4184, 05 2000.

[14] J. Shen, P. Catrysse, and S. Fan, "Mechanism for designing metallic metamaterials with a high index of refraction," *Physical review letters*, vol. 94, p. 197401, 06 2005.

[15] D. Smith, D. Schurig, M. Rosenbluth, S. Schultz, S. A. Ramakrishna, and J. Pendry, "Limitations on subdiffraction imaging with a negative refractive index slab," *Applied Physics Letters*, vol. 82, pp. 1506–1508, 03 2003.

[16] M. Silveirinha and N. Engheta, "Tunneling of electromagnetic energy through subwavelength channels and bends using epsilon-near-zero materials," *Physical review letters*, vol. 97, p. 157403, 11 2006.

[17] W. Yang and M. Fiddy, "Negative refraction does not make perfect lenses," 06 2013.

[18] M. Freire and R. Marques, "A planar magnetoinductive lens for 3d subwavelength imaging," *Applied Physics Letters*, vol. 86, 04 2005.

[19] S. Maslovski, S. Tretyakov, and P. Alitalo, "Near-field enhancement and imaging in double planar polariton-resonant structures," *Journal of Applied Physics*, vol. 96, 11 2003.

[20] M. Silveirinha and C. Fernandes, "Superlens made of a metamaterial with extreme effective parameters," *Physical Review B*, vol. 78, pp. 1–7, 11 2008.

[21] M. Silveirinha, C. Medeiros, and C. Fernandes, "Experimental verification of broadband superlensing using a metamaterial with an extreme index of refraction," *Physical Review B*, vol. 81, pp. 1–4, 01 2010.

[22] P. Belov, Y. Zhao, S. Tse, P. Ikonen, M. Silveirinha, C. Simovski, S. Tretyakov, Y. Hao, and C. Parini, "Transmission of images with subwavelength resolution to distances of several wavelengths in the microwave range," *Physical Review B*, vol. 77, pp. 193 108–1, 05 2008.

[23] P. Belov, Y. Hao, and S. Sudhakaran, "Subwavelength microwave imaging using an array of parallel conducting wires as a lens," *Phys. Rev. B*, vol. 73, p. 033108, 01 2006.

[24] M. Silveirinha, P. Belov, and C. Simovski, "Sub-wavelength imaging at infrared frequencies using an array of metallic nanorods," *Physical Review B*, vol. 75, 10 2006.

[25] T. A. Morgado and M. G. Silveirinha, "Transport of an arbitrary near-field component with an array of tilted wires," *New Journal of Physics*, vol. 11, no. 8, p. 083023, 08 2009. [Online]. Available: https://doi.org/10.1088%2F1367-2630%2F11%2F8%2F083023

[26] M. C. K. Wiltshire, J. V. Hajnal, J. B. Pendry, D. J. Edwards, and C. J. Stevens, "Metamaterial endoscope for magnetic field transfer: near field imaging with magnetic wires," *Opt. Express*, vol. 11, no. 7, pp. 709–715, 04 2003. [Online]. Available: http://www.opticsexpress.org/abstract.cfm?URI=oe-11-7-709

[27] T. Morgado, J. Costa, and M. Silveirinha, "Magnetic uniaxial wire medium," *Physical Review B*, vol. 93, p. 075102, 02 2016.

[28] Cst studio suite. Accessed: 2021-06-04. [Online]. Available: https://www.3ds.com/products-services/simulia/products/cst-studio-suite/

[29] Exotic phenomena in helical-shaped wire metamaterials: from imaging and sensing to topological protection helicalmeta. https://www.it.pt/Projects/Index/4658. Accessed: 2021-05-29.

[30] T. Morgado, G. João, R. Pereira, D. Fernandes, and S. Lannebère, "Experimental demonstration of subwavelength imaging using a helical-shaped wire medium lens," 2 2021.

[31] M. Silveirinha, "Design of linear-to-circular polarization transformers made of long densely packed metallic helices," *Antennas and Propagation, IEEE Transactions on*, vol. 56, pp. 390–401, 02 2008.

[32] T. A. Morgado, S. I. Maslovski, and M. G. Silveirinha, "Uniaxial indefinite material formed by helical-shaped wires," *New Journal of Physics*, vol. 14, no. 6, p. 063002, 06 2012. [Online]. Available: https://doi.org/10.1088/1367-2630/14/6/063002

[33] A. C. Newell, "Error analysis techniques for planar near-field measurements," *IEEE Transactions on Antennas and Propagation*, vol. 36, 1988.

[34] M. LLC. Matlab home. [Online]. Available: https://www.mathworks.com/products/matlab-home.html

[35] J. Marcos, "Medição do campo próximo de antenas e outras estruturas," *ISCTE*, 2011.

[36] "What is a vector network analyzer and how does it work?" https://www.tek.com/document/primer/what-vector-network-analyzer-and-how-does-it-work, accessed: 2021-07-21.